

## Stereotaxic probabilistic maps of the magnocellular cell groups in human basal forebrain

Laszlo Zaborszky<sup>a,\*</sup>, L. Hoemke<sup>b</sup>, H. Mohlberg<sup>b</sup>, A. Schleicher<sup>c</sup>, K. Amunts<sup>b,d</sup>, K. Zilles<sup>b,c</sup>

<sup>a</sup> Center for Molecular and Behavioral Neuroscience, Rutgers, The State University of New Jersey, Newark, NJ 07102, USA

<sup>b</sup> Institute of Neuroscience and Biophysics, INB-3, Medicine, Research Center Juelich, JARA, Juelich, Germany

<sup>c</sup> C. and O. Vogt Institute of Brain Research, Heine University, Duesseldorf, Germany

<sup>d</sup> Rheinisch-Westfaelische Technische Hochschule, RWTH Aachen University, Department of Psychiatry and Psychotherapy, JARA, Aachen, Germany

### ARTICLE INFO

#### Article history:

Received 15 November 2007

Revised 12 May 2008

Accepted 23 May 2008

Available online 7 June 2008

### ABSTRACT

The basal forebrain contains several interdigitating anatomical structures, including the diagonal band of Broca, the basal nucleus of Meynert, the ventral striatum, and also cell groups underneath the globus pallidus that bridge the centromedial amygdala to the bed nucleus of the stria terminalis. Among the cell populations, the magnocellular, cholinergic corticopetal projection neurons have received particular attention due to their loss in Alzheimer's disease. In MRI images, the precise delineation of these structures is difficult due to limited spatial resolution and contrast. Here, using microscopic delineations in ten human postmortem brains, we present stereotaxic probabilistic maps of the basal forebrain areas containing the magnocellular cell groups. Cytoarchitectonic mapping was performed in silver stained histological serial sections. The positions and the extent of the magnocellular cell groups within the septum (Ch1–2), the horizontal limb of the diagonal band (Ch3), and in the sublenticular part of the basal forebrain (Ch4) were traced in high-resolution digitized histological sections, 3D reconstructed, and warped to the reference space of the MNI single subject brain. The superposition of the cytoarchitectonic maps in the MNI brain shows the intersubject variability of the various Ch compartments and their stereotaxic position relative to other brain structures. Both the right and left Ch4 regions showed significantly smaller volumes when age was considered as a covariate. Probabilistic maps of compartments of the basal forebrain magnocellular system are now available as an open source reference for correlation with fMRI, PET, and structural MRI data of the living human brain.

© 2008 Elsevier Inc. All rights reserved.

### Introduction

The basal forebrain comprises heterogeneous structures located close to the medial and ventral surfaces of the cerebral hemispheres. The most prominent feature of the primate basal forebrain is the presence of continuous collection of aggregated and non-aggregated, large, hyperchromic neurons, often referred to as the “magnocellular basal forebrain system” (Hedreen et al., 1984). Compact cell clusters, especially those underneath the posterior limb of the anterior commissure and subpallidal (sublenticular) areas, are called the basal nucleus of Meynert. Large neurons in this area are continuous with similar cells in the medial septum and in the nuclei of the diagonal band and with scattered large cells in association with various fiber bundles, including the internal capsule and anterior commissure. A substantial proportion of the magnocellular neurons in primates represent cholinergic

corticopetal projection neurons (Mesulam et al., 1983; Saper and Chelimsky, 1984; Mesulam and Geula, 1988) that have received particular attention due to their loss in Alzheimer's and related disorders (Perry et al., 1984; Price et al., 1986). Cholinergic neurons in rodents are intermingled with GABAergic, and glutamatergic corticopetal neurons and various peptidergic interneurons (reviewed in Zaborszky and Duque, 2003; Hur and Zaborszky, 2005).

The term basal nucleus of Meynert<sup>1</sup> has been used in the past as a synonym with the substantia innominata (“Unge-nante Mark-Substanz”, Reil, 1809), especially in the clinical literature. This latter term, however, lost its significance in the light of recent tracer and histochemical studies indicating that the main part of the basal forebrain that was previously called the substantia innominata belongs to nearby and better defined anatomical systems. The rostral, subcommissural

\* Corresponding author. Fax: +1 973 353 1588.

E-mail address: [laszloz@andromeda.rutgers.edu](mailto:laszloz@andromeda.rutgers.edu) (L. Zaborszky).

<sup>1</sup> Because of the lack of agreements on the definition of basal nucleus of Meynert or the substantia innominata, when describing the various compartments of the magnocellular neurons, we will use topographical terms and well known fiducial markers.

part of the substantia innominata is mainly occupied by the ventral extensions of the striatum and globus pallidus, i.e. the ventral pallidum and the core/shell subdivisions of the nucleus accumbens (ventral striatum). More caudally, the sublenticular part of the substantia innominata is occupied by the “extended amygdala”, which refers to the subpallidal cell bridges extending from the centromedial amygdala to the bed nucleus of the stria terminalis (Heimer et al., 1985, 1991; Zaborszky et al., 1985; Sakamoto et al., 1999; Heimer et al., 1999; Heimer, 2000; Riedel et al., 2002; de Olmos, 2004; Heimer and van Hoesen, 2006).

Electrophysiological studies in rodents lend support to the notion that basal forebrain cholinergic and GABAergic neurons are important modulators of cortical activation (reviewed in Detari, 2000; Zaborszky and Duque, 2003; Lee et al., 2005). Furthermore, a substantial amount of experimental data in animals, including primates, suggest the involvement of the basal forebrain in attention, learning, memory, reward and cortical plasticity (Wilson and Rolls, 1990; Richardson and DeLong, 1991; Voytko et al., 1994; Chiba et al., 1995; Everitt and Robbins, 1997; Wang et al., 1997; Gaffan et al., 2002; Muir et al., 1994; Conner et al., 2005; Turchi et al., 2005; Sarter et al., 2006; McGaughy et al., 2002; Weinberger 2007). Similarly, imaging studies in humans – as detailed below – lend support for a role of the basal forebrain in a range of cognitive functions. Table 1 lists some of the imaging studies that reported coordinates with reference to the Talairach system (Talairach and Tournoux, 1988).

Paus et al. (1997) investigated the time course of changes in brain activity during a continuous performance auditory vigilance task. As the level of vigilance is shifted from high alert to drowsiness, regional cerebral blood flow (rCBF) decreased in the fronto-parietal network and in several subcortical structures, including the substantia innominata, medial thalamus, and ponto-mesencephalic tegmentum. These changes were interpreted by Paus et al. (1997) as coordinated functions of a separate cortical-subcortical arousal system and a cortical auditory attention network. In the study of Morris et al. (1998), conditioning-related, frequency-specific modulation of tonotopic responses in the auditory cortex of young male volunteers was studied. The modulated regions of the auditory cortex co-varied positively

with activity in the basal forebrain, amygdala, and orbito-frontal cortex. Furthermore, in an aversive conditioning paradigm, Morris et al. (1997) manipulated the salience of visual stimuli and found that augmented activation of the right pulvinar co-varied with a region of the basal forebrain.

It has been long known that basal forebrain lesions in humans, including those from trauma, tumor, or rupture of the anterior cerebral or anterior communicating arteries result in impaired memory functions (Damasio et al., 1985; Morris et al., 1992; Diamond et al., 1997; Abe et al., 1998). Since multiple anatomic regions were often damaged in these cases, it has been difficult to determine the exact area of the lesion that caused the cognitive symptoms. A recent fMRI study in young male volunteers suggested that activity in the nucleus of the diagonal band of Broca and the subcallosal area is related to episodic memory recall (Fujii et al., 2002). In another study, using delayed match to sample paradigm sensitive for working memory, activations were found in the dorsolateral prefrontal cortex and basal forebrain regions (Swartz et al., 1995).

Cocaine infusion into cocaine-dependent volunteers leads to significant fMRI signal changes in a basal forebrain region that is populated by cholinergic cells (Breiter and Rosen, 1999). However, the same region has been claimed as part of the “sublenticular extended amygdala”, a continuum between the centromedial amygdala and the bed nucleus of the stria terminalis (Heimer and Van Hoesen, 2006). It remains an open question whether or not activations related to the basal forebrain corticopetal system can be segregated from those cell groups that belong to the extended amygdala system.

Finally, consistent with the state-dependent changes of unit recordings in rodents across sleep stages (e.g., Lee et al., 2005), basal forebrain areas in humans were among those that showed significant changes in glucose metabolism (rCMRglu) or rCBF throughout the sleep–wake cycle (Braun et al., 1997; Maquet et al., 1997; Nofzinger et al., 2002).

Due to the complex anatomy of the basal forebrain, the contribution of a specific anatomical system to a particular cognitive function has not been well understood. The superimposition of postmortem anatomical and *in vivo* functional data into the same reference space allows correlations

**Table 1**

Neuroimaging studies reporting significant effect in the substantia innominata-diagonal band with specific coordinates in the Talairach space

Author	Region as defined by the authors	X	Y	Z	Comment
Paus et al. (1997)	Substantia innominata	24	6	–15	Significant negative co-variations of rCBF with time on-task, PET
		23	6	–15	CBF co-variations with CBF in the left thalamus, PET
Morris et al. (1997)	Basal forebrain	12	–10	–8	rCBF, in an aversive classical conditioning the BF region co-varied with the right pulvinar, PET
Braun et al. (1997)	Basal forebrain (AH-POA)	–2	–8	–4	rCBF: SWS vs pre-sleep W, PET
		4	–6	–8	rCBF: REM vs SWS, PET
		4	2	4	rCBF: SWS vs post-sleep W, PET
Maquet et al. (1997)	Basal forebrain	2	2	–4	Decreased rCBF during SWS, PET
Morris et al. (1998)	Basal forebrain	–10	–10	–2	rCBF, Discriminatory aversive auditory conditioning, PET,
	Basal forebrain	8	–2	–12	
Fujii et al. (2002)	N. diagonal band of Broca	–3	5	–6	rCBF, Episodic memory retrieval, PET
De Rosa et al. (2004)	Medial septum/diagonal band	8	7	–7	Proactive interference in a discriminatory associative learning paradigm, fMRI
	Ventral striatum	14	–2	–2	

AH-POA=anterior hypothalamic-preoptic area.

BF=basal forebrain.

CBF=cerebral blood flow.

rCBF=regional cerebral blood flow.

REM=rapid eye movement sleep.

SWS=sleep wave sleep.

W=wake.

**Table 2**

Brains used for spatial normalization of basal forebrain areas

ID	Age	Sex	Postm. delay (h)	Shrinkage factor <sup>a</sup>	Brain weight (g) <sup>b</sup>	Cause of death
14686	37	Male	24	2.02	1150	Heart failure
2431	39	Male	10	2.32	1264	Drowning
1696	54	Male	8	2.44	1547	Myocardial infarct
28193	68	Male	16	2.12	1198	Vascular disease
20784	75	Male	24	2.15	1200	Toxic glomerulonephritis
38281	59	Female	24	2.05	947	Cardio-respiratory insufficiency
5694	72	Female	12	1.82	1071	Renal failure
6895 <sup>c</sup>	79	Female	16	1.47	1164	Cardio-respiratory insufficiency
54491 <sup>c</sup>	79	Female	24	1.93	1174	Carcinoma of the bladder
295 <sup>c</sup>	85	Female	14	1.67	923	Mesenteric artery infarction

<sup>a</sup> Defined as the ratio between the estimated fresh volume and its volume after histological processing. This factor was used for volume correction in Table 4 (see Amunts et al., 2005).

<sup>b</sup> Brain weight after fixation.

<sup>c</sup> Fixed in Bodian, all other brains were fixed in formalin.

between cerebral microstructure and functional imaging data (Rolland and Zilles, 1994; Amunts et al., 2002; Zilles et al., 2002; Amunts et al., 2004). A microstructural map of the basal forebrain region, however, is not available. Therefore, the goal of the present study was to provide cytoarchitectonic probabilistic 3D maps of basal forebrain structures that contain cholinergic projection neurons. Since cholinergic neurons are often aggregated in clusters and constitute most of the large neurons (>20  $\mu\text{m}$  long axis) in this brain area (Mesulam et al., 1983), the areas containing such magnocellular cell groups within the septum, the horizontal and vertical limbs of the diagonal band, and in the sublenticular basal forebrain can be easily delineated in histological sections stained with a modified Gallyas's silver method for cell bodies (Merker, 1983). This method has been proven as an excellent marker for cytoarchitectonic studies (Uylings et al., 1999; Zilles et al., 2002). The cytoarchitectonic maps of ten human brains were warped to the reference space of the Montreal Neurological Institute (MNI) single subject brain (Collins et al., 1994; Holmes et al., 1998). The resulting probabilistic maps can now be correlated with functional neuroimaging data for a better understanding of the role of various basal forebrain systems in cognitive functions.

## Materials and methods

### Fixation, MRI and histological processing

Brains from five males and five females with no record of neurological or psychiatric diseases were obtained at autopsy (Table 2). All subjects were included in the body donor program of the Institute of Anatomy at the University of Duesseldorf (Germany). The mean age of the subjects was: 64.9 years (range 37–75 years, Table 2). Seven brains were fixed in 4% formaldehyde for several months; three brains were fixed in Bodian-fixative. The brains were suspended at the basilar artery to avoid compression during fixation. T1-weighted MRI scans were obtained using a 1.5 T Siemens Magnetron SP scanner (3D FLASH pulse sequence; flip angle=40°; TR=40 ms; TE=5 ms; voxel size=1.17 mm [mediolateral]×1 mm [rostrocaudal]×1 mm [dorsoventral]) for documentation of brain size and shape before subsequent histological processing, which induces shrinkage and distortion.

The brains were dehydrated in graded alcohols, embedded in paraffin, and sectioned coronally (20  $\mu\text{m}$  whole brain sections). Images of the paraffin block-faces were obtained after each 15th section. Each 15th section was mounted on a gelatin-coated slide and stained for cell bodies with a modified silver method of Gallyas (Merker, 1983). This staining yields high contrast of cell bodies for cytoarchitectonic analysis and delineation of regions of interest. Each stained section was digitized using a flat bed scanner.

### Delineation of basal forebrain areas in the histological sections, spatial normalization and generation of probabilistic maps

The outlines of various basal forebrain compartments were traced on 2D images of the sections (1.2 mm apart) with a final resolution of 7000×6000 pixels using in-house software. The outlines were processed as contour line for each histological section. For delineation of the magnocellular basal forebrain compartments we used a modified version of the Ch1–Ch4 nomenclature of Mesulam (Mesulam et al., 1983), as detailed in the Results section. Magnocellular neurons in the basal forebrain often constitute cell aggregates or clusters that facilitate their recognition. As a rule, borders of delineated areas were drawn where the number of large cells precipitously diminished toward surrounding regions (e.g. Fig. 5B).

The histological sections of the postmortem brains were reconstructed in 3D ("histological volume") from the digitized histological sections using the MRI scans of the fixed brain as a shape reference with a resolution of 1 mm isotropic. A major difficulty of the reconstruction results from inevitable distortions of the histological sections, which occur during cutting and mounting on glass carriers: These distortions were modelled by the reconstruction algorithm, to arrange the histological sections correctly within the MR volume of the fixed brain (Schormann and Zilles 1998; Hoemke, 2006).

Each 3D reconstructed histological volume was spatially normalized to the single subject T1-weighted MNI reference brain (Collins et al., 1994; Holmes et al., 1998) using a combination of affine linear and non-linear, elastic transformations (Henn et al., 1997; Hoemke, 2006). The MNI reference space is frequently used in functional imaging studies, e.g. in the software environment of SPM (<http://www.fil.ion.ucl.ac.uk/spm/>). The origin of this reference space is not aligned to the intersection of the AC-PC line with the interhemispheric plane as in the Talairach stereotaxic space (Talairach and Tournoux 1988; T-T). To obtain a stereotaxic space with the origin of the anterior commissure at the level of the interhemispheric plane, the present data were shifted in Y and Z plane by 4 and 5 mm, respectively ("anatomical MNI

**Table 3**Centers of gravity of cytoarchitectonic areas in the anatomical MNI space<sup>a</sup>

Cytoarchitectonic area	X <sup>b</sup>	Y <sup>b</sup>	Z <sup>b</sup>
Ch1–2L <sup>c</sup>	−1.8	3.7	−2.0
Ch1–2R <sup>c</sup>	3.0	4.3	−2.5
Ch3L	−6.0	2.0	−6.7
Ch3R	7.5	2.1	−6.9
Ch4L	−17.2	−2.3	−7.1
Ch4R	18.2	−1.5	−6.3
Ch4pL	−23.9	−8.6	−4.8
Ch4pR	24.0	−9.3	−4.5

<sup>a</sup> See definition in Materials and methods.

<sup>b</sup> In mm.

<sup>c</sup> L,R left, right side.



**Table 4**

Mean volumes of the basal forebrain structures in mm<sup>3</sup> with standard deviations (N=10) using individual correction for shrinkage<sup>a</sup>

Structure	Left hemisphere	Right hemisphere
Ch1_2	45.02±29.90	51.09±26.75
Ch3	23.21±16.15	22.75±13.88
Ch4	85.03±36.26	89.73±36.65
Ch4p	30.36±16.84	27.51±16.72
CH_all	183.62±49.22	191.08±55.22

Neither interhemispheric or gender differences were significant ( $p>0.05$ ).

<sup>a</sup> Individual shrinkage factor see Table 2.

space"; Amunts et al., 2005). Note that the coordinates are not in the T-T space, but in the anatomical MNI space.

Finally, based on the whole 3D brain reconstructions, volume and shape of the magnocellular cell groups were computed. We applied therefore the transformations, which have been calculated for the 3D-reconstruction of the whole histological sections, for the contour lines. Since the spatial resolution of the digitized histological sections (and the contour lines) was larger than that of the MR data set of the postmortem brain (reference for 3D-reconstruction), we decreased the resolution of the contours accordingly. In the next step, a stack of filled contour lines was generated, which was visualized by surface rendering techniques (marching cube approach). In this study, the software Amira<sup>®</sup> (Mercury Computer Systems<sup>®</sup>, Chelmsford, USA) was applied for this purpose.

Probability maps were calculated separately for each Ch compartment. Based on the sample of ten brains, they describe the relative frequency with which the same basal forebrain area (e.g., Ch1–2; Ch3, Ch4, or Ch4p) was repre-

sented in each voxel of the reference space as shown in Fig. 8 for Ch1–2, Fig. 9 for Ch3, Fig. 10 for Ch4, and Fig. 11 for the posterior part of Ch4 compartment. Fig. 12 shows the probability maps of the Ch space in the reference brain without subdividing into several compartments. The center of gravity for each Ch compartments was then calculated (Table 3). For a spatial comparison of the Ch cell groups with the surrounding BF structures, including the ventral pallidum, nucleus accumbens and the bed nucleus of the stria terminalis, all structures were combined in one data set by assigning labels to each voxel. A voxel was assigned to a structure that had the highest probability or that exceeded a threshold of 40% (Fig. 13). The generation of these maximum probability maps (MPM) is described elsewhere (Eickhoff et al., 2005, 2006). Histograms were calculated for quantifying the volume of overlap of the individual structures (Fig. 14). Since the absolute volume of overlap is larger in large nuclei and smaller in small nuclei, we normalized the histograms by the sum of voxels to make the histograms comparable for all nuclei (see Supplementary Table 1 for the original data). Fig. 16 shows the 3D rendering of an individual brain using the software Amira<sup>®</sup>.

### Volume measurements

The volumes of the individual Ch compartments (Table 4) were calculated using Cavalieri's principle as previously described (Amunts et al., 2005). Volumes of Ch1–2, Ch3, Ch4 and Ch4p were analyzed statistically with respect to left–right and sex differences (ANOVA with repeated-measures design; within factors: area, and hemisphere; between factor: sex). A

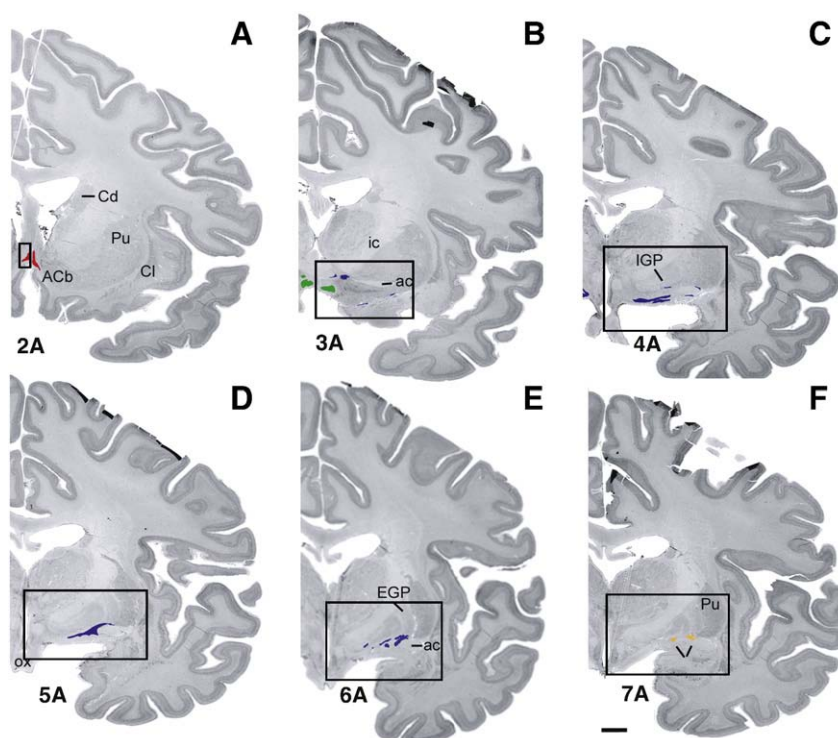


**Fig. 1.** Low magnification series of coronal sections from rostral (A) to caudal (F) from a male subject (#1696) stained with the Merker (1983) method to show the location of magnocellular basal forebrain cell groups in relation to other brain structures. The various Ch cell groups as delineated on the images of the sections are color-coded: Ch1–2: red; Ch3: green; Ch4: blue and Ch4p: beige. Ch4p group is marked by two lines in panel (F). Delineated areas are blown up in subsequent figures. Numbered letters under each panel refer to the corresponding figure. ACb, nucleus accumbens; ac, anterior commissure; Cd, caudate nucleus; Cl, claustrum; EGP, external globus pallidus; IGP, internal globus pallidus; ic, internal capsule; ox, optic chiasm; Pu, putamen. Bar scale: 5 mm.

significance level of  $\alpha=0.05$  was set for all tests. Age was used as a covariate. Bonferroni correction was used to control for the alpha error.

## Results

### *Diagonal band of Broca and basal nucleus of Meynert in histological sections*

Fig. 1 shows the position of all magnocellular compartments as delineated in this study from a male brain #1696 at six coronal levels. Figs. 2–7 illustrate the cytoarchitecture of the delineated areas as traced from high resolution images of the same sections shown in Fig. 1.

#### *Ch1–Ch2 compartment (Figs. 1A, 2A, B)*

Magnocellular neurons at the level of the area subcallosa and gyrus rectus stretching from just below the fused midline of the septum to the ventral edge of the brain and extend close to the medial border of the nucleus accumbens. This compartment largely corresponds to the medial septal nucleus and the nucleus of the diagonal band of Broca as defined by Andy and Stephan (1968). In the more dorsal part of this area, corresponding to the Ch1 group of Mesulam et al. (1983), the cell bodies and initial dendrites of the neurons tend to be oriented perpendicularly to the crossing fibers of the anterior commissure in coronal sections. The ventral part of this compartment (Ch2 group of Mesulam) merges laterally with the Ch3 cell groups. No distinction was made between Ch1 and Ch2 groups.

#### *Ch3 group (Figs. 1B, 3A, B)*

The Ch3 group of the present account corresponds to the horizontal nucleus of the diagonal band of Broca as defined by Hedreen et al., (1984), labeled by DB in Halliday et al. (1993) and Saper (2004) and labeled with DBB in Swaab (2003). The Ch3 compartment can be regarded as linking cell groups in the medial septum-vertical diagonal band nucleus (Ch1–2) with the more elaborate magnocellular cell groups in the sub-lenticular forebrain (Ch4). Fig. 3A is taken at the level where the fibers of the anterior commissure reached the opposite side through the midline, to show the characteristic position of the Ch3 group. The cells in this compartment (Fig. 3B) tend to be oriented in all directions and are somewhat looser arranged than the more laterally located, often fusiform cells of the Ch4 cell groups (compare Fig. 3B with Fig. 4B).

#### *Ch4 group (Figs. 1C–E, 3A, 4–6)*

Cell aggregates in the subpallidal region, largely correspond to the basal nucleus of Meynert as defined by Vogels et al. (1990) and De Lacalle et al. (1991). We did not differentiate subcomponents of the Ch4 compartment as suggested by Mesulam et al. (1983). The large neurons in the Ch4 compartment extend as far rostrally as cell aggregates underneath the nucleus accumbens (Fig. 3A). Large aggregates of darkly stained cell group within the ventrolateral edge of the bed nucleus of the stria terminalis at the border of the internal capsule/anterior commissure were also classified as Ch4 (Fig. 3A). Fig. 4A, taken at the rostral level of the supraoptic nucleus where darkly stained cells of the Ch4 group are present in the area ventral to the internal part of the globus pallidus, stretching between the lateral hypothalamus and the temporal aspect of the anterior

commissure, some large neurons are in close relation to the anterior commissure. Neurons often build cell clusters and their nuclei are oriented more or less parallel to the brain surface (Fig. 4B). Fig. 5A is taken slightly more caudally, at the level of the anterior hypothalamic area. The delineated area contains scattered large neurons, in addition to cell

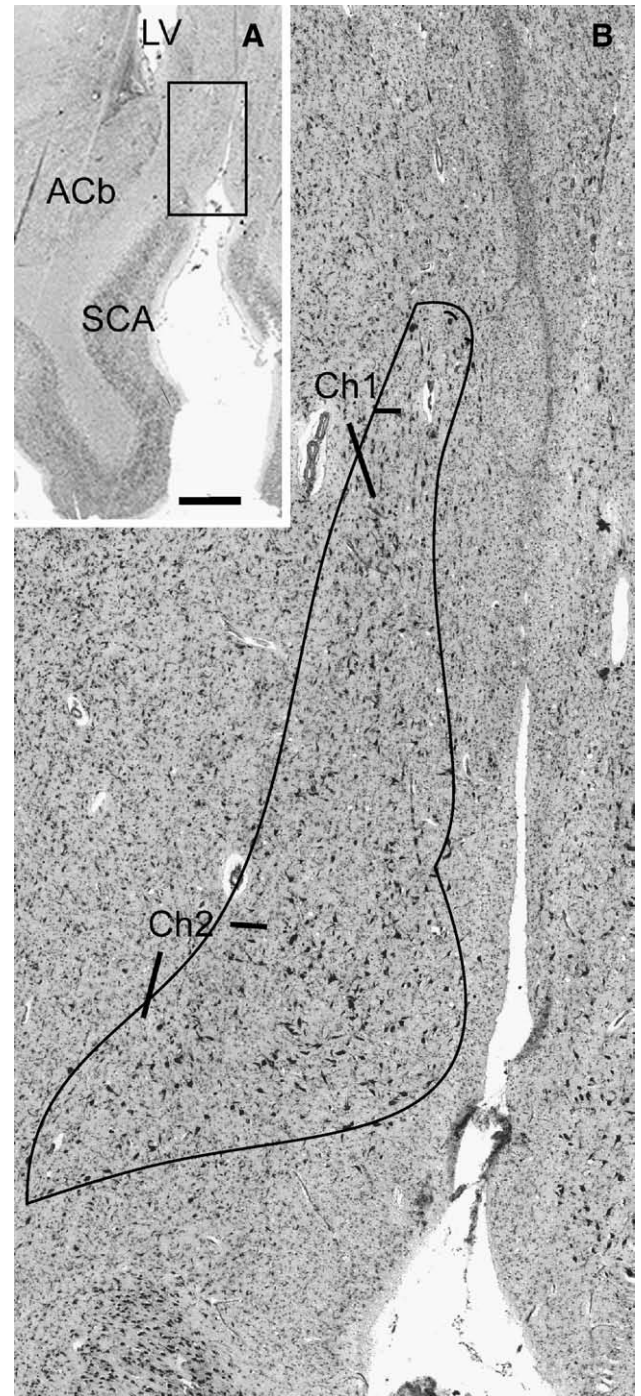


**Fig. 2.** Septum-diagonal band complex (Ch1–2 groups). (A) Low magnification to show the septal region. Box outlines the approximate area enlarged in (B). (B) High magnification from panel A to demonstrate the cytoarchitecture of the Ch1–2 groups. The delineated area from the high-resolution image of the section roughly corresponds to the original traced region shown with red in the box of Fig. 1A. Note that in the dorsal part of this area the cells are smaller and oriented vertically (Ch1), while in more ventral parts, the neurons are larger without apparent orientation (Ch2). ACb, nucleus accumbens; LV, lateral ventricle; SCA, subcallosal area. Bar scale in (A): 2 mm for (A), 240  $\mu$ m for (B).



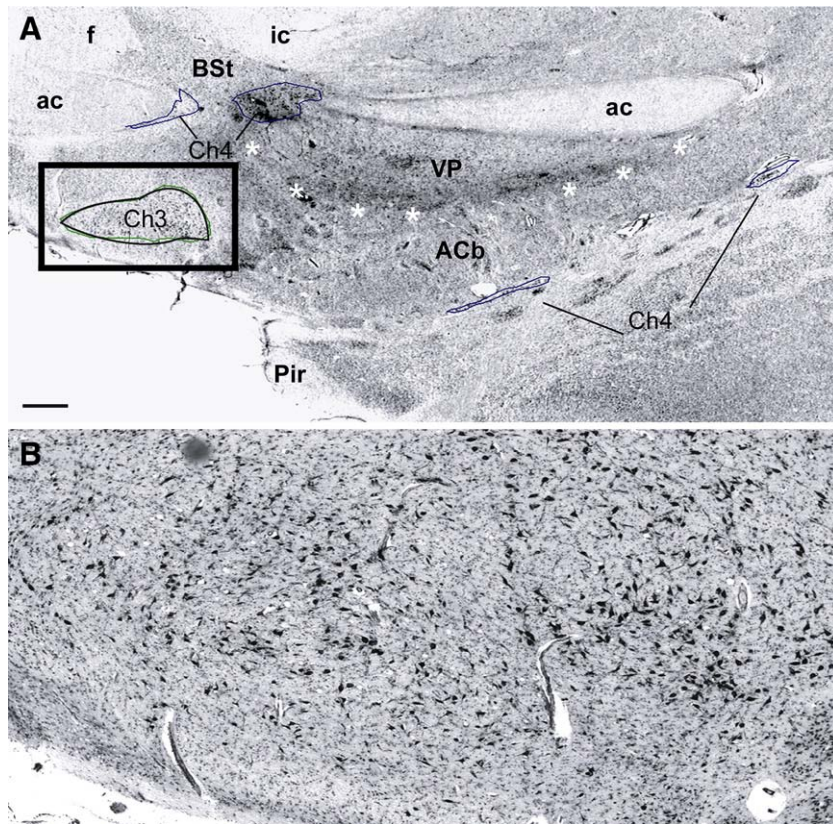


**Fig. 3.** (A) The Ch3 cell group (boxed area) and the lamellar-like protrusions of the Ch4 groups underneath of the nucleus accumbens. The large aggregate of darkly stained cell group within the ventrolateral corner of the bed nucleus of the stria terminalis (BSSt) was also classified as Ch4. Panel A depicts the same section as shown in Fig. 1B at higher magnification. The original green tracing used for the Ch3 group in the boxed area in (A) is reinforced with black line. This level is characterized by the crossing fibers of the anterior commissure (ac). The ventral border of the ventral pallidum (VP), that can be recognized with the naked eye as a shiny tissue area to its high iron content, is marked with white asterisks. Panel B is a high resolution image from the boxed area in panel A. Magnocellular neurons of the Ch3 group are loosely arranged between the fibers of the diagonal band showing a variety of orientations. Pir, piriform cortex; f, fornix. Bar scale in (A): 1 mm for (A), 175  $\mu$ m for (B).

clusters of various sizes. Fig. 6 is from a more caudal level, showing small clusters of Ch4 neurons ventral to the globus pallidus and medial and dorsal to the temporal limb of the anterior commissure. Some of these cell groups are arranged around the ansa peduncularis.

#### Ch4 posterior group (Figs. 1F, 7)

We retained the term Ch4p for magnocellular cell groups in a well-defined area that begins caudal to the supraoptic nucleus at the level where the optic tract adjoins the internal capsule/cerebral peduncle and extends progressively laterally up to the most caudal level of the medial mammillary nucleus and the central nucleus of the amygdala. Fig. 7B is an enlarged view of the medial, triangular cell aggregate of Ch4p from Fig. 7A, which is located underneath the internal component of the globus pallidus. At the level of the subthalamic nucleus, a few large, darkly stained cells invade the medial aspect of the putamen, the lateral part of the globus pallidus, and the area above the central amygdaloid nucleus (not shown). These small cell clusters also belong to Ch4p.

#### Probabilistic maps

The probabilistic maps of Figs. 8–11 show the interindividual microstructural variability for each delineated Ch compartment using a color code: blue colour shows that only one brain is represented in an actual voxel, while red color indicates that all ten brains are overlapping. Those parts

of the Ch 1–2 that have the lowest inter-subject variability (i.e., highest overlap of individual brain structures) are located rostrally and immediately adjoining the crossing fibers of the anterior commissure ( $y=3$  to  $y=0$ ). Approximately 28% of the voxels in the Ch1–2 region in the reference brain represent overlap of five or more brains (Fig. 8).

Fig. 9 shows the probabilistic map of the Ch3 cell groups, which are located more posterior than the Ch1–2 compartment. It reveals a slightly higher intersubject variability than Ch1–2. Most of the voxels representing a high overlap of Ch3 cells are found between levels  $y=0$  and  $y=-3$ . Approximately 24% of all voxels in Ch3 represent an overlap of five or more brains.

The probabilistic maps of the Ch4 region show a relatively large overlap at  $y=-6$  (Fig. 10). However, a few voxels with high overlap stretch rostrally in front of the decussating fibers of the anterior commissure (between  $y=0$  and  $y=-3$ ). Approximately 28% of all voxels in the Ch4 region in the reference brain represent an overlap of five or more brains.

The Ch4p region shows the highest inter-subject variability among the delineated structures, accordingly only few red voxels can be seen in Fig. 11. This compartment occupies the most caudal position among the magnocellular basal forebrain structures. On the average, 19% of all voxels in the Ch4p of the reference space overlap in five or more brains.

Fig. 12 displays probabilistic maps at 6 coronal levels when all Ch groups are considered without subdividing into compartments. Since neighboring Ch compartments overlap



at their borders, these maps show many more red voxels that originate from all ten brains than the previous probabilistic maps of the individual compartments. Fig. 13 shows the maximum probability maps (MPM) of the various Ch regions. Each voxel was assigned to the cytoarchitectonic area that showed the greatest overlap (“winner take all”) among the ten examined post-mortem brains. As a result, MPMs show a non-overlapping representation of the Ch compartments in the anatomical MNI space.

Fig. 14 shows the normalized distributions of overlapping voxels of the individual Ch regions in the anatomical MNI space. The comparison of the frequency distributions of these basal forebrain structures clearly demonstrates a similar degree of intersubject variability across Ch compartments (see for original data [Supplementary Table 1](#)).

#### Volume measurements

The mean volume of the whole Ch1–4 complex was 191 mm<sup>3</sup> on the right side and 184 mm<sup>3</sup> on the left side

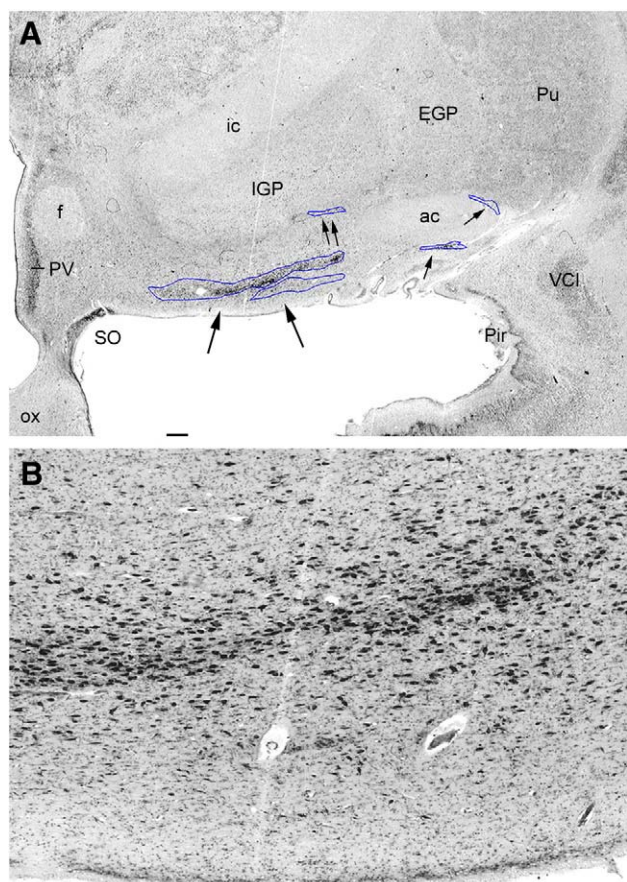


**Fig. 4.** Coronal section at the level of the anterior hypothalamic area with the Ch 4 cell groups in the sublentiform tissue. The supraoptic (SO) and the neurosecretory cells of the paraventricular hypothalamic nucleus (PV) along the third ventricle are stand out with their large, darkly stained neurons. Large delineated area in the sublentiform gray with several smaller cell groups belonging to the Ch4 cell groups around the posterior limb of the anterior commissure are visible (single arrows). A small Ch4 cell group along the ventral border of the globus pallidus is labeled by double arrow. (A) The same section as Fig. 1C with the original tracing. (B) Area from panel (A), large arrows at the bottom of the section in (A) indicate the approximate field enlarged in (B). Note the magnocellular cells are oriented parallel with the ventral surface of the brain. EGP, external pallidum; f, fornix; IGP, internal globus pallidus; ic, internal capsule, ox, optic chiasm; Pir, piriform cortex; Pu, putamen; VCI, ventral claustrum. Bar scale in (A) 1 mm for (A), 115  $\mu$ m for (B).

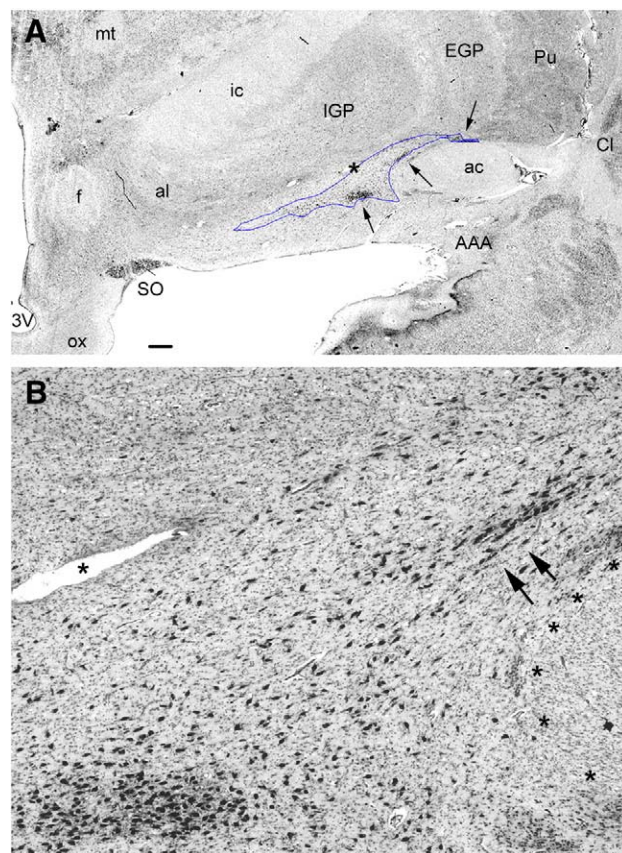


**Fig. 5.** Coronal section, approximately 3.6 mm caudal to Fig. 4. Delineated area belongs to the Ch4 compartment in the sublentiform gray. (A) The same section as Fig. 1C with the original tracing. Arrows point to a large (medially) and two smaller cell clusters. (B) An enlargement from panel A to show the cytoarchitecture of the Ch4 group at this level. Double arrows point to the small cell cluster near the medial aspect of the temporal limb of the anterior commissure (labeled by asterisks). The large cell cluster from (A) is located in the lower left corner of this panel. Note the loose arrangement of large cells between these two cell clusters and the fact that the number of large, darkly stained cells rapidly diminish dorsally towards the globus pallidus, allowing a clear demarcation of the Ch4 cell groups from the rest of the brain. al, ansa lenticularis. Asterisk in (A) and (B) mark the same vessel as fiducial marker. Scale bar: in (A) 1 mm for (A) and 100  $\mu$ m for (B).

(Table 4). Among the compartments, the Ch4 group had the largest volume while the Ch3 constituted the smallest one. Interhemispheric and sex related differences in volume were not significant ( $p > 0.05$ ). There was, however, a significant age effect: both left and right Ch4 showed a negative correlation with age ( $\alpha = 0.05$ ) using ANOVA with a repeated measures design and Bonferroni correction (Fig. 15).

#### 3D Rendering

Fig. 16 displays surface rendering of case #1696 to illustrate the spatial distribution of cell clusters in more detail. Although the full configuration can be appreciated only when rotating the model in a coordinate system with surrounding structures, it is obvious even from these panels, showing various aspects of the model, that the entire magnocellular system occupies a complicated space, extending from medially in the septum to caudo-laterally toward the amygdaloid body. Within this space, magnocellular neurons of the Ch4 compartment form several bands (clusters) of various size and shape that are in part parallel and in part connected with each other. The cell aggregates of the Ch3, and especially Ch1–2 have a simpler



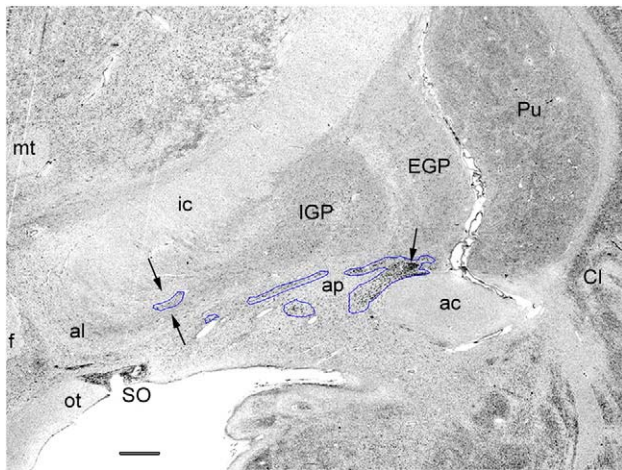


**Fig. 6.** Coronal section at the caudal level of the supraoptic hypothalamic nucleus (SO). Note several delineated cell groups of the Ch4 compartment underneath the inner (IGP) and external segments (EGP) of the globus pallidus. One small cell cluster is embedded in the medial aspect of IGP, near the fibers of the internal capsule (between arrows). Same section as Fig. 1E with the original tracing. The ansa peduncularis (ap) passes through the Ch4 cell groups. Inside of the large delineated island of the Ch4 cell group that is attached to the medial aspect of the anterior commissure an arrow points to a cell cluster. f, fornix; mt, mammillothalamic tract; ot, optic tract. Scale bar: 1 mm.

configuration. If other structures were added to this rendering it becomes obvious that the various cell aggregates of the Ch4 compartment penetrate the nucleus accumbens, ventral pallidum, and the bed nucleus of the stria terminalis to some extent.

## Discussion

In the present study, we manually delineated the magnocellular cell aggregates of the human basal forebrain in silver-stained sections in order to generate cytoarchitectonic probabilistic maps in stereotaxic space. Most of the neurons of the extended amygdala are small or medium-sized and occupy a different position than the cholinergic neurons in the subcommissural/subpallidal territory in primates (Ghashghaei and Barbas, 2001). Since most of the cholinergic neurons are larger than cells in the surrounding areas, and 90% of the magnocellular perikarya in the Ch4 compartment are cholinergic (Mesulam et al., 1983), the space identified based upon the presence of large neurons in high-resolution histological sections, is likely represent the cholinergic space; i.e., the volume occupied by the cortically

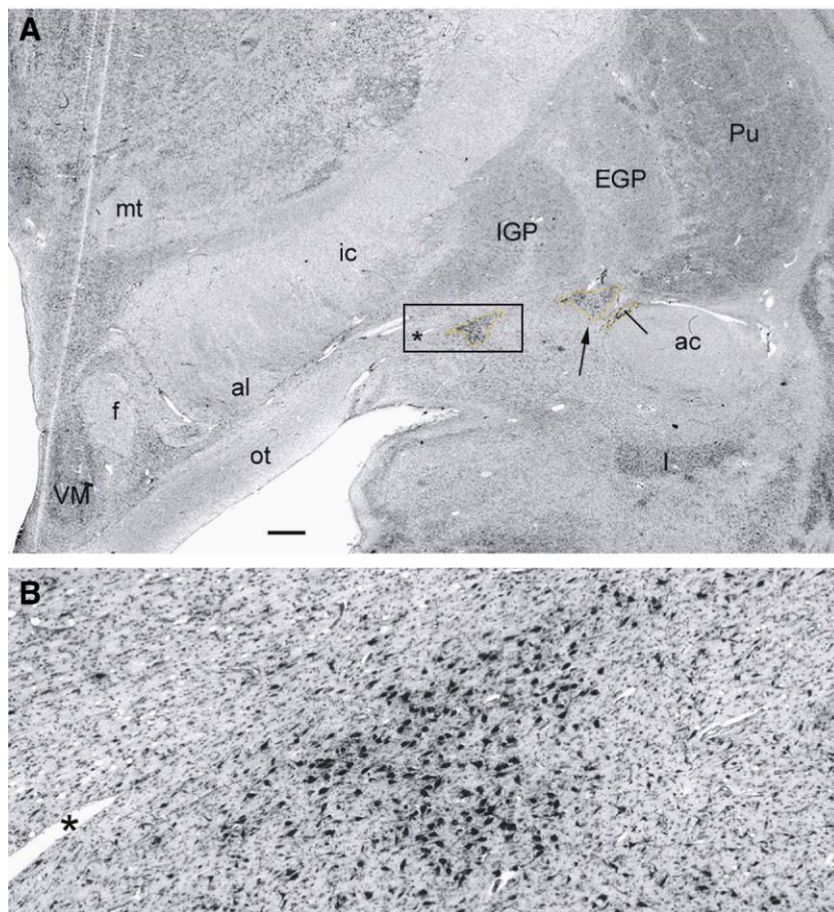


**Fig. 7.** Coronal section through the posterior portion of the Ch4 complex (Ch4p) at the level of the ventromedial hypothalamic (VM) nucleus. The same section as Fig. 1F. The boxed area with a large cell cluster is enlarged in panel B. Since Ch4p was traced originally with beige color that is poorly visible, another large cell aggregate is marked with an arrow. A small cell cluster attached to the dorsomedial surface of the anterior commissure is labeled by a solid line in (A). Asterisk marks the same vessel in (A) and (B) for orientation. ot, optic tract; I, intercalated cell nucleus of the amygdala. Scale bar: in (A) 1 mm for (A) and 75  $\mu$ m for (B).



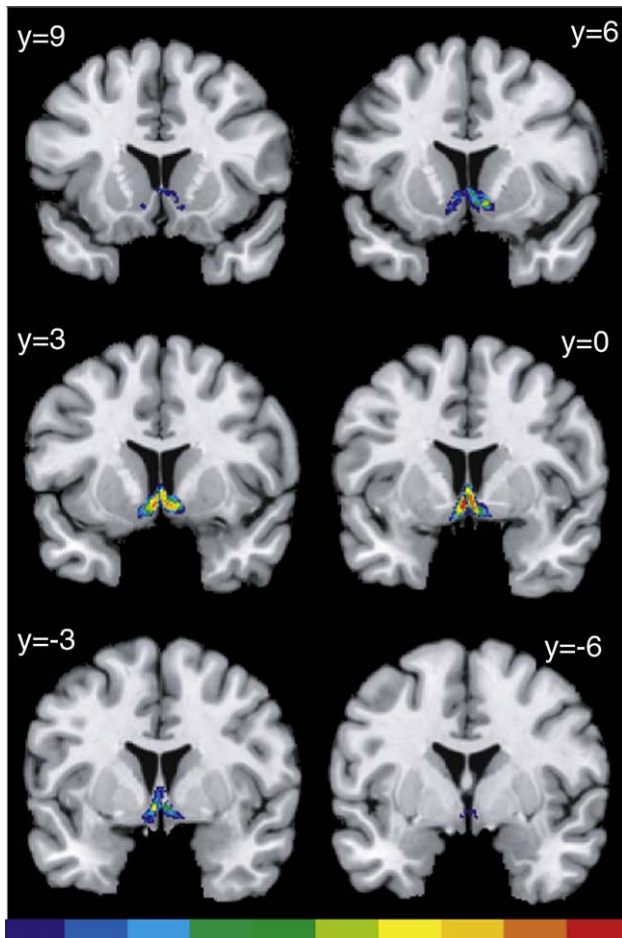


**Fig. 8.** Probabilistic maps of the Ch1–2 cell groups in the anatomical MNI space. The y coordinates indicate distances from the anterior commissure in mm in the rostro-caudal directions. The left hemisphere is left in the image. The frequency with which the actual anatomical structure is overlapped in the sample of ten brains is color coded. The scale at the bottom of this figure indicates the degree of overlap in each voxel. The blue areas show that only one brain is represented with its actual structure, red color shows that all ten brains are overlapping. Voxels representing ten brains are located between levels  $y=3$  and  $y=0$ .

projecting cholinergic cell bodies. Mapping from ten brains resulted in probabilistic maps with high overlap, comparable to other subcortical nuclei (e.g., amygdala; Amunts et al., 2005). The resulting probabilistic maps can be correlated with future functional neuroimaging data for a better understanding of the role of various basal forebrain systems in cognitive functions.

### Organization of the human magnocellular basal forebrain system

The widely dispersed, more or less continuous collection of aggregated and non-aggregated large neurons that extend obliquely from the septum rostrally to the level of the lateral geniculate body caudally is often called the “magnocellular basal nucleus” (Saper and Chelimsky, 1984; De Lacalle and Saper, 1997), or “magnocellular basal forebrain system” (Hedreen et al., 1984). The rostral portion of these neurons is associated with the medial septum and the nucleus of the diagonal band of Broca, and primarily project to the hippocampus. On the other hand, neurons located more caudally in the subcommissural and sublenticular space, often referred to as the basal nucleus of Meynert, project topographically to various cortical areas (Jones et al., 1976; Mesulam et al., 1983; Pearson et al., 1983). The topographical organization of corticopetal cholinergic projection in humans has been confirmed in cases of Alzheimer’s disease that had relatively selective cell loss in various sectors of the basal forebrain. From these cases one can conclude that medial frontal and cingulate cortices are innervated from more medial cell groups, whereas the lateral neocortex, including the prefrontal, temporal, parietal and occipital cortices receive their projections from more lateral subdivisions of the magnocellular system (Arendt et al., 1985; Mesulam and Geula, 1988).

Mesulam et al. (1983) proposed a Ch nomenclature to differentiate cholinergic neurons according to their cortical target areas. According to this scheme the entire Ch4 space is subdivided into 6 compartments termed anteromedial (Ch4am), anterolateral (Ch4al), anterointermediate (Ch4ai), intermediodorsal (Ch4id), intermedioventral (Ch4ai) and posterior (Ch4p). However, the original subdivisions in standardized MRI space were only partly applied in the present study because we did not apply specific staining for cholinergic neurons. Moreover, in many instances it is not possible to consistently define boundaries between individual compartments, as noted already in 1988 in a symposium on nomenclature of the basal forebrain cholinergic system (Butcher and Semba, 1989). For example, the boundaries between Ch1 and Ch2 seem to be arbitrary and these two regions were taken together in our study, similar to the delineations used by Vogels et al. (1990). The Ch3 group, according to the original description of Mesulam et al. (1983), refers to a band of fusiform neurons close to the ventral surface of the brain in the subcommissural area (see for example, Figs. 7A and 10A in Mesulam and Geula, 1988; Fig. 3A

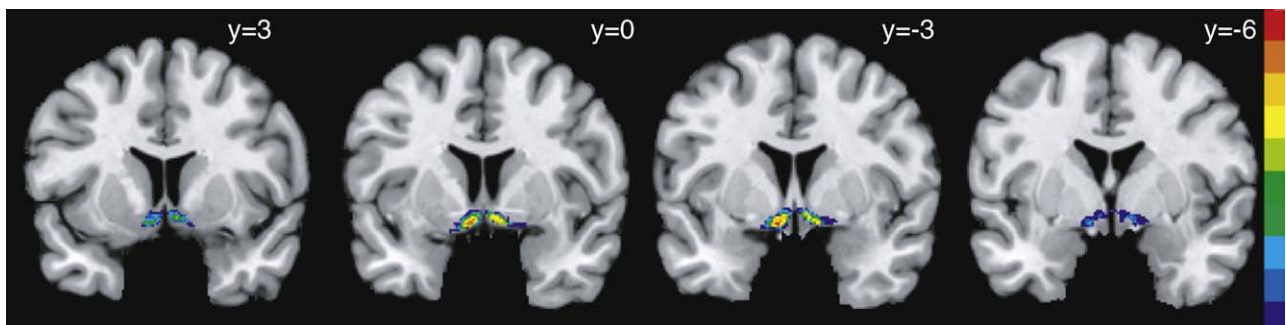


**Fig. 9.** Probabilistic maps of the Ch3 cell groups at four rostro-caudal levels. The scale at right of this figure indicates the degree of overlap in each voxel. Same color code as in Fig. 8. Note that voxel representing maximum overlap are located between levels  $y=0$  and  $y=-3$ .

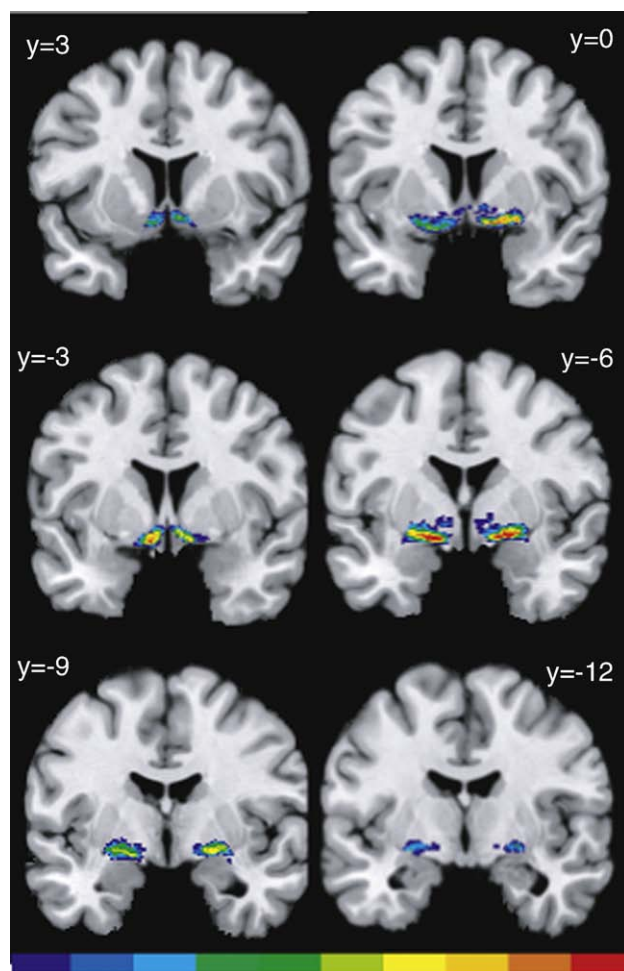


**Fig. 10.** Probabilistic maps of the Ch4 cell groups at six rostro-caudal levels. Color code is the same as in Figs. 8, 9. Note that most of the voxels representing maximum overlap (ten brains) are located at level  $y=-6$ .

in Mufson et al., 1988). The cell group designated as Ch3 in our paper represents a transitory area between the septum-diagonal band complex and the more caudal cell groups of the magnocellular basal forebrain system and may correspond to be part of the anteromedial Ch4 group in some publications (Mesulam et al., 1983; Lehericy et al. 1993; Gilmor et al., 1999). We, and others, noted that a separation of the anterior Ch4 group into medial and lateral sectors by a vascular structure, as proposed by Mesulam and his coworkers, is ambiguous due to the variation of the vessels (Halliday et al., 1993; Swaab, 2003). Similarly, delineations of other Ch4 subdivisions are

difficult to reproduce due to lack of specific landmarks, except for a well-defined posterior subgroup behind the supraoptic nucleus where the optic tract attaches to the internal capsule/cerebral peduncle. Our Ch4p probably corresponds to the nucleus subputaminalis of Ayala (Ayala, 1915; Simic et al., 1999). Hyperchromic, large neurons can often be found underneath the nucleus accumbens, and around the borders of the posterior limb of the anterior commissure along the putaminal border or more caudally within the ventral putamen itself. We incorporated these cell groups into the Ch4 group, since these cells seem to be connected to the bulk of Ch4 cell aggregates in 3D renderings.

The inhomogeneous, dense clusters of neurons in the magnocellular basal complex are interrupted by regions of low cellular density in humans (Halliday et al., 1993) as well as in rodents and monkeys (Zaborszky et al., 1999). The heterogeneous distribution of cholinergic cells and the highly variable shape of the cholinergic space across the rostrocaudal extent of the basal forebrain may have contributed to differing renderings of the magnocellular basal forebrain complex in primates, including humans (see Pearson et al., 1983; Mesulam et al., 1986; Ulfing, 1989). A publication of a preliminary computer-assisted 3D reconstruction of the magnocellular cells from gallocytin-stained human sections by Heinsen and his colleagues (2006) showed a similar configuration as depicted in Fig. 16 of the present paper. Moreover, the magnocellular space in humans as shown in Fig. 16 in this study is remarkably similar in its architecture to the cholinergic space in computerized 3D reconstructions of rodents (Zaborszky et al., 1999; Nadasdy and Zaborszky, 2000; Zaborszky et al., 2005).

#### *Intersubject variability in standard reference space*

Obstacles to a more thorough examination of basal forebrain structures in imaging studies of the living human brain include the low intensity and interdigitating nature of the different anatomical systems. In addition, variations in the size of the ventricles and the exact angle of brain orientation may affect the assessment of ventral areas in MRI. In an attempt to overcome these problems, Buchsbaum et al. (1998) took advantage of the thin-plate spline warping technique, developed by Bookstein (1990) using geometrical landmarking, including the anterior commissure, the internal capsule, and the fornix that are easily identifiable in MRI scans. However, because the positions of the magnocellular cell groups differ across brain sections, a 2D warping method seriously limits the conclusions that can be reached using this method for evaluating the magnocellular

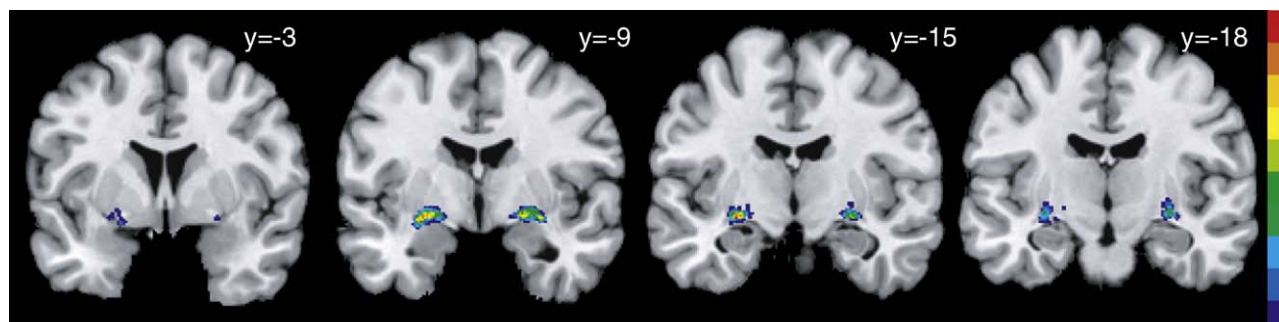


**Fig. 11.** Probabilistic maps of the Ch4p cell groups at four rostro-caudal levels. Note the paucity of red voxels, indicating that most of the voxels originate from individual brains.



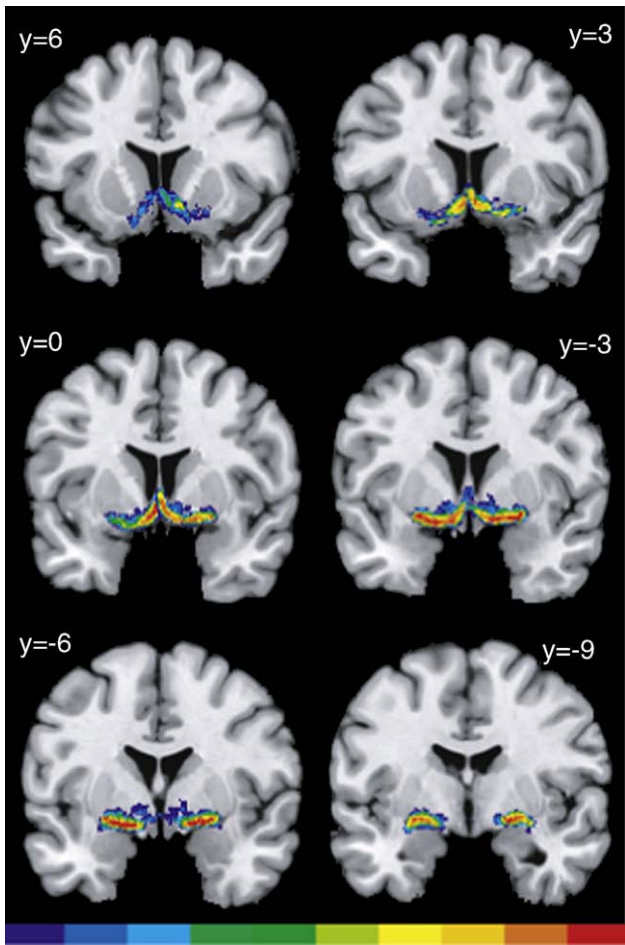


**Fig. 12.** Probabilistic maps showing all Ch groups without divisions into different compartments. Note that these maps show many more red voxels than previous maps of individual compartments due to the fact that the individual Ch compartments overlap at their borders. Same color code as Figs. 8–11.

basal forebrain complex. Moreover, some structures like the ventral border of nucleus accumbens have indistinct margins that are difficult to trace on MRI images.

The method employed here overcomes these problems. The magnocellular cell groups are identified in high resolution histological sections with an appropriate staining. The 3D reconstruction of the histological sections allows for the transfer of delineated structural information into 3D MRI space. The spatial normalization of the postmortem brains to the common reference space, which consists of several steps, enables to study differences between the architecture of the individual brains and the reference brain. The affine linear transformations reduce global differences in scaling (size), rotation (orientation), translation (position), and shearing. The subsequent non-linear transformations were pixel/voxelwise transformations that account for local differences in brain shape. The modeling of the MR data sets of each brain as an elastic medium ensures that the non-linear transformations were smooth. Hence, the topology of the brain regions was preserved.

Variability in the probabilistic maps is, therefore, mainly an indicator for interindividual structural variability on a microscopic level rather than gross brain morphology. Normalizing the overlapping voxels to the total volume of a particular Ch compartments suggests that the intersubject variability of the four Ch regions is similar (Fig. 14). Intersubject variability can be expressed in various ways, for example, we can compare the

percentage of voxels in the probability maps that represent more than five brains (see [Supplementary Table 1](#)). Taken all of Ch compartments together (volume for one hemisphere in MNI space: 4785 mm<sup>3</sup>), the Ch volume that originates from five or more brains is 37% of the total. This percentage value is compatible to that of the amygdala (44%; [Amunts et al., 2005](#)). It exceeds that for the previously studied neocortical area 44 and area 45 of Broca's regions (11% and 18%, respectively; [Amunts et al., 1999](#)). Another example of a neocortical area is sensory area 3b, which is represented in the anatomical MNI space by a volume of 107,514 mm<sup>3</sup>, however; only 16% of this space is devoted to overlapping voxels originating from five or more brains ([Eickhoff et al., 2005](#)). Due to relatively high overlap (i.e., low interindividual variability) of subcortical structures, as compared to some neocortical areas, probability maps should be efficient tools for the precise topographical analysis of structural changes in the basal forebrain in aging and Alzheimer's disease.

#### *Age and disease-related changes in the magnocellular basal complex*

Severe involvement of the magnocellular basal complex has been found in Alzheimer's disease, where various studies reported cell loss up to 90% ([Whitehouse et al., 1981](#); [Vogels et al., 1990](#); [Lehericy et al., 1993](#); [Cullen and Halliday, 1998](#)). Estimations of the neuronal loss of basal nucleus of Meynert during normal aging also vary greatly from 23% to 50% to no neuronal loss at all ([Whitehouse et al., 1981](#); [Chui et al., 1984](#);

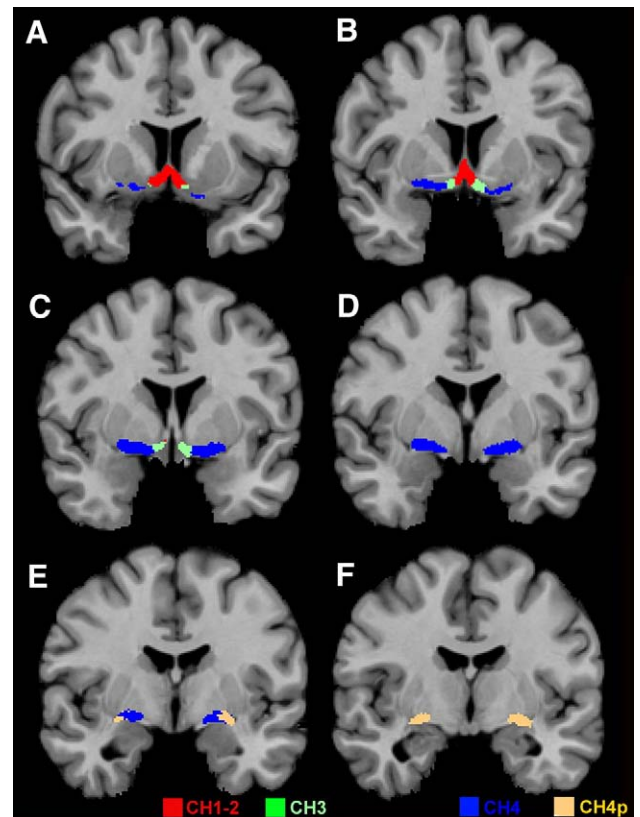


**Fig. 13.** Maximum probability maps (MPMs) of all Ch groups in the anatomical MNI space (A, rostral; F, caudal). In the MPM each voxel is assigned to the cytoarchitectonic compartment that showed the greatest overlap among the ten examined brains. Note the colors represent individual Ch compartments, similarly as in Fig. 1, and not the degree of overlap as in Figs. 8–12. Red: Ch1–2 cell groups; green: Ch3; blue: Ch4; beige: Ch4p. In this figure the left hemisphere is right.

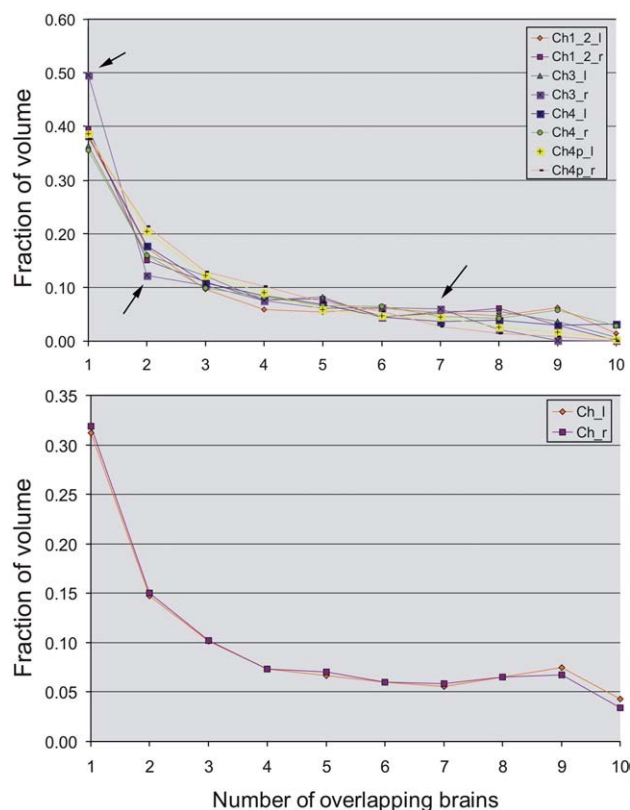


**Fig. 14.** Frequency distribution of the various Ch4 cell groups showing the relation of overlapping volumes in the anatomical MNI space. In order to make the distributions of the various Ch compartments with different volumes comparable for all nuclei, we normalized the histograms by the sum of voxels (for original data see [Supplementary Table 1](#)). Upper histogram displays the individual Ch compartments, lower histogram show the total left and right Ch space only. For example, the total volume of right Ch3 compartment is represented in the MNI space by 856 mm<sup>3</sup>, from this volume 424 voxels (424 mm<sup>3</sup>) originates from single brains, thus occupying 49.5% of the total space dedicated to Ch3; 105 voxels originate from 2 brains (12.3%) and 51 voxels from seven brains (5.9%). For easier orientation, these percentage values are marked by arrows in the upper diagram. The lower diagram shows only the distribution of voxels from the total left and right Ch compartments, respectively. For example, the total volume of the right Ch space in the MNI reference brain is represented by 4855 voxels (4855 mm<sup>3</sup>), from this volume 166 mm<sup>3</sup> represent overlapping space from 10 brains, while 1549 mm<sup>3</sup> devoted to Ch space originating from single brains (for more details see [Supplementary Table 1](#)).

[De Lacalle et al., 1991](#)). In addition to Alzheimer's disease, there are structural changes in the basal forebrain occasionally in Parkinson's disease, Rett syndrome, progressive supranuclear

palsy, Parkinson dementia complex of Guam, dementia pugilistica, Pick's disease, Korsakoff's syndrome, Down syndrome, Wernicke's encephalopathy, and Cretzfeldt-Jacob disease (reviewed in [Swaab, 2003](#)). However, much controversy remains whether or not the neuropathological changes are primary or secondary, what is the time course of changes, and whether or not the neuropathological changes occur in the entire extent of the cholinergic space or are restricted to its specific regions. Some of the unresolved issues are at least partly due to the fact that neuropathological examinations are restricted to postmortem cases from a single time point of advanced stages of the disease.

*In vivo* measures of morphological changes in the basal forebrain would be of great importance for a better understanding of how structural changes correlate to cognitive symptoms in Alzheimer's disease. These measures are difficult to obtain since smaller subdivisions of the basal forebrain cannot be distinguished *in vivo* in routine MRI, but at a microscopic resolution. An alternative to an identification of microstructural nuclei in the individual brain, geometrical landmarks have often defined volumes of interest of the magnocellular basal forebrain cell groups. For example, age-related gray matter loss in the basal forebrain was reported in a voxel-based MRI study ([Ishii et al., 2005](#)). However, it is not clear from this study to what extent shrinkage of other brain areas contributed to the result. In two another studies, [Sasaki et al. \(1995\)](#) and [Hanyu et al. \(2002\)](#) measured the thickness of an area below the anterior commissure in coronal MR images in patients with Alzheimer's disease and elderly controls. They found a significant correlation between age and thickness of the measured values in control subjects, in agreement with the age-dependent decrease of the volume of Ch4 in our study. However, methodological problems may have influenced the results of this study. For example, a signal loss in the globus pallidus, caused by its magnetic susceptibility effect with the T2-weighted spin-echo sequence ([Schenker et al., 1993](#)), may limit the dorsal delineation of the ROI. Furthermore, in linear measurements the angle of the section plane affects the thickness of the tissue. In another study, [Teipel et al. \(2005\)](#) defined an ROI about 20 times larger than the Ch4 area in our study that included the anterior commissure, large parts of the ventral globus pallidus and a small part part of the medioventral putamen in addition to Ch4 of present account. [Teipel et al. \(2005\)](#) found a signal decrease in proton density MRI in this ROI in patients with Alzheimer's disease compared with healthy

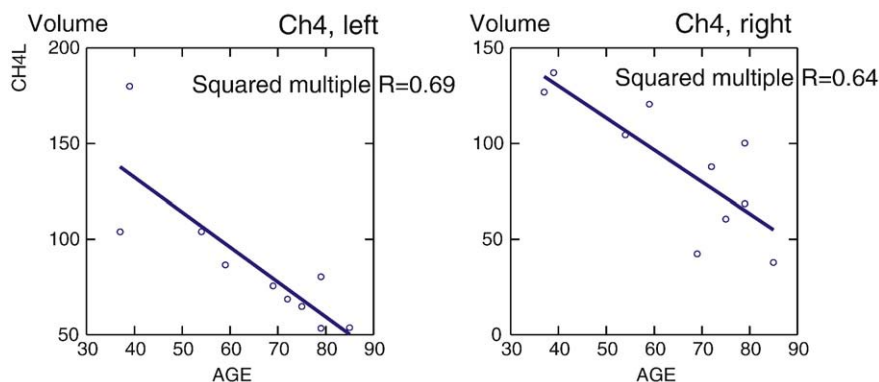


**Fig. 15.** Plots showing the correlation between age and volume of the Ch4 left and Ch4 right groups. Both the left and right Ch4 compartments showed a negative correlation with age ( $\alpha=0.05$ ) using ANOVA with a repeated measures design.



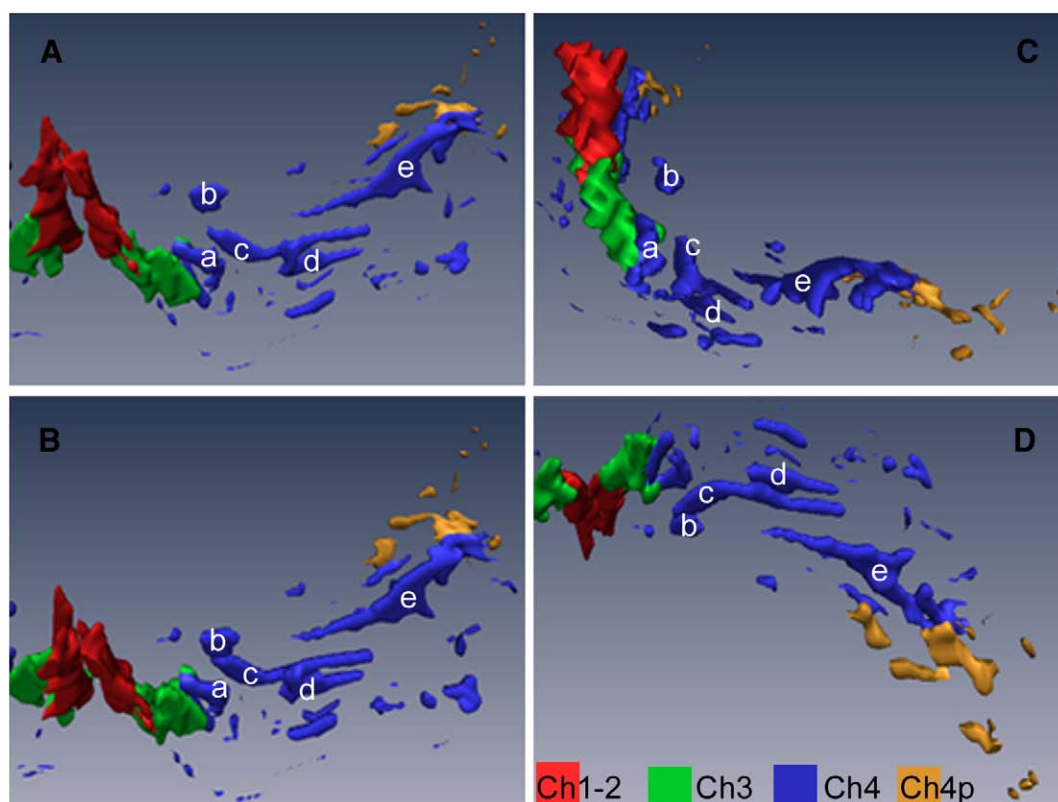


**Fig. 16.** Computer-assisted (Amira<sup>®</sup>) 3D reconstruction of the Ch1–4 cell groups of the right hemisphere of the same case shown in the histological sections of Figs. 1–7 (case #1696). The various Ch compartments are color-coded. (A and B) Coronal view with two different angles inclined towards the viewer. (C) Lateral view, (D) aspect from below. The Ch4 (blue) compartment consists of various size and shaped bands or clusters that are in part parallel and in part are associated each other. For better orientation, some of the larger clusters are arbitrarily termed with letters *a–e*. Note that clusters *b* and *c* of the Ch4 compartment are attached to each other in panels B and D but are separated in (A) and (C), however, compartments *c* and *d* are in all aspects grown together. The Ch1–2 (red) and the Ch3 (green) compartments show simpler 3D configurations. The posterior Ch4 compartments (yellow) consist of several smaller clusters that are partially covered by the Ch4 cell groups (primarily by cluster *e*) in panels A–C but are clearly visible from a ventral aspect (D).

subjects. The degree of signal decline was related to the degree of grey matter atrophy in cortical areas. However, taking into consideration that many neighboring structures of the magnocellular space were included, the measurements based on such large ROIs may lead to erroneous conclusions. Future research is needed to validate these findings.

### Concluding remarks

Probabilistic maps of the magnocellular cell groups in standardized stereotaxic space can provide the fine-grained parcellation necessary to localize neuropathological changes in a heterogeneous region such as the basal forebrain. The ability to delineate precisely microstructural details together with the improved sensitivity of advanced MRI, and with neuropsychological battery for memory disorders should allow the identification of patients with mild cognitive impairment, a patient population who will convert to Alzheimer's disease, but in which early intervention may slow the disease progress.

Probabilistic maps from neighboring basal forebrain areas, including the ventral pallidum, nucleus accumbens, and the bed nucleus of the stria terminalis, will soon be available (Voss, Amunts, Zilles and Zaborszky, in preparation). Using an anatomical toolbox integrated in the SPM program the superimposition of postmortem anatomical and *in vivo* functional data in the same space of a reference brain allows correlations to be made between microstructural details and functional imaging data (Eickhoff et al., 2005). The anatomical volume of interest can be defined by using the maximum probability maps

or thresholding of individual probabilistic maps (e.g., >50%). Calculating the intersection between a volume of activation and anatomically defined volume, hypotheses can be tested and the structural substrates of functional activations can be inferred in a probabilistic context (Eickhoff et al., 2006). For example, it has been hypothesized, based upon anatomical data, that specific clusters of projection neurons in the basal forebrain together with specific prefrontal and posterior cortical associational regions constitute distributed elements of functional parallel circuits (Zaborszky, 2002). The close connective relationship between prefrontal and basal forebrain regions in rodents and in primates are well known (Sesack et al., 1989; Ghashghaie and Barbas, 2001; Golmayo et al., 2003; Spiga and Zaborszky, 2006), and imaging and neurophysiological studies have found neural correlates of both top-down [task-driven] and bottom-up [stimulus-driven] attention processes in frontal and posterior parietal cortices (Buschman and Miller, 2007). However, it is not known whether or not the cholinergic system is activated as part of a general arousal system or if spatially specific cholinergic and other basal forebrain compartments would be correlated with activations in specific cortical targets. Such knowledge is critical for a better understanding of the directionality of information flow in attentional networks.

### Acknowledgments

This project was supported by PHS/NINDS grant NS023945 to L.Z. The Human Brain Project/Neuroinformatics research was funded jointly by the National Institute of Mental Health,

NINDS, the National Institute of Drug Abuse, the National Cancer Center (KZ and KA), the Helmholtz Gemeinschaft (KZ and KA), and by the Bundesministerium für Bildung und Forschung, Brain Imaging Center West (KZ). The authors thank Dr. Susan Feldman for providing with constructive criticisms of a previous version of this article.

## Appendix A. Supplementary data

Supplementary data associated with this article can be found, in the online version, at doi:10.1016/j.neuroimage.2008.05.055.

## References

- Abe, K., Inokawa, M., Kashiwagi, A., Yanagihara, T., 1998. Amnesia after a discrete basal forebrain lesion. *J. Neurol. Neurosurg. Psychiatry* 65, 126–130.
- Amunts, K., Schleicher, A., Burgel, U., Mohlberg, H., Uylings, H.B.M., Zilles, K., 1999. Broca's region revisited: Cytoarchitecture and intersubject variability. *J. Comp. Neurol.* 412, 319–341.
- Amunts, K., Schleicher, A., Zilles, K., 2002. Architectonic mapping of the human cerebral cortex. *Conceptual Advances Brain Res.* Taylor and Francis, Inc., New York, NY, pp. 29–52.
- Amunts, K., Weiss, P.H., Mohlberg, H., Pieperhoff, P., Eickhoff, S., Gurd, J.M., Marshall, J.C., Shah, N.J., Fink, G.R., Zilles, K., 2004. Analysis of neural mechanisms underlying verbal fluency in cytoarchitectonically defined stereotaxic space – the roles of Brodmann areas 44 and 45. *NeuroImage* 22, 42–56.
- Amunts, K., Kedo, O., Kindler, M., Pieperhoff, H., Mohlberg, H., Shah, N.J., Habel, U., Schneider, F., Zilles, K., 2005. Cytoarchitectonic mapping of the human amygdala, hippocampal region and entorhinal cortex: intersubject variability and probability maps. *Anat. Embryol.* 210, 343–352.
- Andy, O.J., Stephan, H., 1968. The septum in the human brain. *J. Comp. Neurol.* 133, 383–410.
- Arendt, T., Bigl, V., Tennstedt, A., Arendt, A., 1985. Neuronal loss in different parts of the nucleus basalis is related to neuritic plaque formation in cortical target areas in Alzheimer's disease. *Neuroscience* 14, 1–14.
- Ayala, G., 1915. A hitherto undifferentiated nucleus in the forebrain (nucleus subputaminalis). *Brain* 37, 433–438.
- Bookstein, F.L., 1990. Distortion correction. In: Toga, A.W. (Ed.), *Three-Dimensional Neuroimaging*. Raven Press, Ltd., New York, pp. 235–249.
- Braun, A.R., Balkin, T.J., Wesensten, N.J., Carson, R.E., Varga, M., Baldwin, P., Selbie, S., Belenky, G., Herscovitch, P., 1997. Regional cerebral blood flow throughout the sleep–wake cycle. An  $H_2^{15}O$  PET study. *Brain* 120, 1173–1197.
- Breiter, H.C., Rosen, B.R., 1999. Functional magnetic resonance imaging of brain reward circuitry in the human. *Ann. New York Acad. Sci.* 877, 523–547.
- Buchsbaum, M.S., Fallon, J.H., Wei, T.-C., Guich, S., Spiegel-Cohen, J., Hamilton, M., Tang, C., 1998. A method of basal forebrain anatomical standardization for functional image analysis. *Psych. Res. Neuroimaging Section* 84, 113–125.
- Buschman, T.J., Miller, E.K., 2007. Top-down versus bottom-up control of attention in the prefrontal and posterior parietal cortices. *Science* 315, 1860–1862.
- Butcher, L.L., Semba, K., 1989. Reassessing the cholinergic basal forebrain: nomenclature, schemata, and concepts. *Trends Neurosci.* 12, 483–485.
- Chiba, A.A., Bucci, D.J., Holland, P.C., Gallagher, M., 1995. Basal forebrain cholinergic lesions disrupt increments but not decrements in conditioned stimulus processing. *J. Neurosci.* 15, 7315–7322.
- Chui, H.C., Bondareff, W., Zarow, C., Slager, U., 1984. Stability of neuronal number in the human nucleus basalis of Meynert with age. *Neurobiol. Aging* 5, 83–88.
- Collins, D.L., Neelin, P., Peters, T.M., Evans, A.C., 1994. Automatic 3D intersubject registration of MR volumetric data in standardized Talairach space. *J. Comput. Assist. Tomogr.* 18, 192–205.
- Conner, J.M., Chiba, A.A., Tuszyński, M.H., 2005. The basal forebrain cholinergic system is essential for cortical plasticity and functional recovery following brain injury. *Neuron* 48, 173–179.
- Cullen, K.M., Halliday, G.M., 1998. Neurofibrillary degeneration and the cell loss in the nucleus basalis in comparison to cortical Alzheimer pathology. *Neurobiol. Aging* 19, 297–306.
- Damasio, A.R., Graff-Radford, N.R., Eslinger, P.J., Damasio, H., Kassel, N., 1985. Amnesia following basal forebrain lesions. *Arch. Neurol.* 42, 263–271.
- De Lacalle, S., Saper, C.B., 1997. The cholinergic system in the primate brain: basal forebrain and pontine-tegmental cell groups. In: Bloom, F.E., Bjorklund, A., Hokfelt, T. (Eds.), *Handbook of Chemical Neuroanatomy: 13. The primate nervous system, part I*. Elsevier Science B. V., pp. 217–262.
- De Lacalle, S., Iraizoz, J., Ma Gonzalo, L., 1991. Differential changes in cell size and number in topographic subdivisions of human basal nucleus in normal aging. *Neuroscience* 43, 445–456.
- de Olmos, J.S., 2004. Amygdala. In: Paxinos, G., Mai, J.K. (Eds.), *The Human Nervous System*, 2nd ed. Elsevier Academic Press, Amsterdam, pp. 739–868.
- De Rosa, E., Desmond, J.E., Anderson, A.K., Pfefferbaum, A., Sullivan, E.V., 2004. The human basal forebrain integrates the old and the new. *Neuron* 41, 825–837.
- Detari, L., 2000. Tonic and phasic influence of basal forebrain unit activity on the cortical EEG. *Behav. Brain Res.* 115, 314–327.
- Diamond, B.J., DeLuca, J., Kelley, S.M., 1997. Memory and executive functions in amnesia and non-amnesic patients with aneurysms of the anterior communicating artery. *Brain* 120, 1015–1025.
- Eickhoff, S.B., Stephan, K.E., Mohlberg, H., Grefkes, C., Fink, G.R., Amunts, K., Zilles, K., 2005. A new SPM toolbox for combining probabilistic cytoarchitectonic maps and functional imaging data. *NeuroImage* 25, 1325–1335.
- Eickhoff, S.B., Heim, S., Zilles, K., Amunts, K., 2006. Testing anatomically specified hypotheses in functional imaging using cytoarchitectonic maps. *NeuroImage* 32, 570–582.
- Everitt, B.J., Robbins, T.W., 1997. Central cholinergic systems and cognition. *Ann. Rev. Psychol.* 48, 649–684.
- Fujii, T., Okuda, J., Tsukiura, T., Ohtake, H., Miura, R., Fukatsu, R., Suzuki, K., Kawashima, R., Itoh, M., Fukuda, H., Yamadori, A., 2002. The role of the basal forebrain in episodic memory retrieval: A positron emission tomography study. *NeuroImage* 15, 501–508.
- Gaffan, D., Easton, A., Parker, A., 2002. Interaction of inferior temporal cortex with frontal cortex and basal forebrain: double dissociation in strategy implementation and associative learning. *J. Neurosci.* 22, 7288–7296.
- Ghashghaie, H.T., Barbas, H., 2001. Neural interaction between the basal forebrain and functionally distinct prefrontal cortices in the rhesus monkey. *Neuroscience* 103, 593–614.
- Gilmer, M.L., Erickson, J.D., Varoqui, H., Hersch, L.B., Bennett, D.A., Cochran, E.J., Mufson, E.J., Levey, A.L., 1999. Preservation of nucleus basalis neurons containing choline acetyltransferase and the vesicular acetylcholine transporter in the elderly with mild cognitive impairment and early Alzheimer's disease. *J. Comp. Neurol.* 411, 693–704.
- Golmayo, L., Nunez, A., Zaborszky, L., 2003. Electrophysiological evidence for the existence of a posterior cortical–prefrontal–basal forebrain circuitry in modulating sensory responses in visual and somatosensory rat cortical areas. *Neuroscience* 119, 597–609.
- Halliday, G.M., Cullen, K., Cairns, M.J., 1993. Quantitation and three-dimensional reconstruction of Ch4 nucleus in the human basal forebrain. *Synapse* 15, 1–16.
- Hanyu, H., Asano, T., Sakurai, H., Tanaka, Y., Takasaki, M., Abe, K., 2002. MR analysis of the substantia innominata in normal aging, Alzheimer disease, and other types of dementia. *AJNR Am. Neuroradiol.* 23, 27–32.
- Hedreen, J.C., Struble, R.G., Whitehouse, P.J., Price, D.L., 1984. Topography of the magnocellular basal forebrain system in human brain. *J. Neuropath. Exp. Neurol.* 43, 1–21.
- Heimer, L., Van Hoesen, G.W., 2006. The limbic lobe and its output channels: implications for emotional functions and adaptive behavior. *Neurosci. Biobehav. Rev.* 30, 126–147.
- Heimer, L., Alheid, G.F., Zaborszky, L., 1985. Basal ganglia. In: Paxinos, G. (Ed.), *The Rat Nervous System*, vol. 1. Academic Press, Sydney, pp. 37–86.
- Heimer, L., de Olmos, J., Alheid, G.F., Zaborszky, L., 1991. "Perestroika" in the basal forebrain: opening the border between neurology and psychiatry. *Progr. Brain Res.* 87, 109–165.
- Heimer, L., de Olmos, J.S., Alheid, G.F., Pearson, J., Sakamato, N., Shinoda, K., Marksteiner, J., Switzer III, R.C., 1999. The human basal forebrain: Part II. In: Bloom, F.E., Bjorklund, A., Hokfelt, T. (Eds.), *The Primate Nervous System*, Part III. *Handbook of Chemical Neuroanatomy*, vol. 15. Elsevier, Amsterdam, pp. 57–226.
- Heimer, L., 2000. Basal forebrain in the context of schizophrenia. *Brain Res. Rev.* 31, 205–235.
- Heinsen, H., Hampel, H., Teipel, S.J., 2006. Response to Boban et al.: computer-assisted 3D reconstruction of the nucleus basalis complex, including the nucleus subputaminalis (Ayala's nucleus). *Brain* 129, E43.
- Henn, S., Schormann, T., Engler, K., Zilles, K., 1997. Elastische Anpassung in der digitalen Bildverarbeitung auf mehreren Auflösungsstufen mit Hilfe von Mehrgitterverfahren. In: Paulus, E., Wahl, F.M. (Eds.), *Mustererkennung*. Springer, Berlin, pp. 392–399.
- Hoemke, L., 2006. A multigrid method for anisotropic PDEs in elastic image registration. In: Falgout, R.D. (Ed.), *Numerical Linear Algebra with Applications*. Wiley InterScience, pp. 215–229.
- Holmes, C.J., Hoge, R., Collins, L., Woods, R., Toga, A.W., Evans, A.C., 1998. Enhancement of MR images using registration for signal averaging. *J. Comput. Assist. Tomogr.* 22, 324–333.
- Hur, E., Zaborszky, L., 2005. Vglut2 afferents to the medial prefrontal and primary somatosensory cortices: a combined retrograde tracing in situ hybridization. *J. Comp. Neurol.* 483, 351–373.
- Ishii, K., Kawachi, T., Sasaki, H., Kono, A.K., Fukuda, T., Kojima, Y., Mori, E., 2005. Voxel-based morphometric comparison between early- and late-onset mild Alzheimer's disease and assessment of diagnostic performance of Z score images. *Am. J. Neuroradiol.* 26, 333–340.
- Jones, E.G., Burton, H., Saper, C.B., Swanson, L.W., 1976. Midbrain, diencephalic and cortical relationship of the basal nucleus of Meynert and associated structures in primates. *J. Comp. Neurol.* 167, 385–420.
- Lee, M.G., Hassani, O.K., Alonso, A., Jones, B.E., 2005. Cholinergic basal forebrain neurons burst with theta during waking and paradoxical sleep. *J. Neurosci.* 25, 4365–4369.
- Lehericy, S., Hirsch, E.C., Cervera-Pierot, P., Hersch, L.B., Bakchine, S., Piette, F., Duyckaerts, C., Hauw, J.-J., Javoy-Agid, F., Agid, Y., 1993. Heterogeneity and selectivity of the degeneration of cholinergic neurons in the basal forebrain of patients with Alzheimer's disease. *J. Comp. Neurol.* 330, 15–31.
- Maquet, P., Degueldre, C., Delfiore, G., Aerts, J., Peters, J.-M., Luxen, A., Franck, G., 1997. Functional neuroanatomy of human slow wave sleep. *J. Neurosci.* 17, 2807–2812.
- McGaughy, J., Dalley, J.W., Morrison, C.H., Everitt, B.J., Robbins, T.W., 2002. Selective behavioral and neurochemical effects of cholinergic lesions produced by



- intrabasal infusions of 192 IgG-saporin on attentional performance in a five-choice serial reaction time task. *J. Neurosci.* 22, 1905–1913.
- Merker, B., 1983. Silver staining of cell bodies by means of physical development. *J. Neurosci. Meth.* 9, 235–241.
- Mesulam, M.-M., Geula, G., 1988. Nucleus basalis (Ch4) and cortical cholinergic innervation in the human brain: observations based on the distribution of acetylcholinesterase and choline acetyltransferase. *J. Comp. Neurol.* 275, 216–240.
- Mesulam, M.-M., Mufson, E.J., Levey, A.I., Wainer, B.H., 1983. Cholinergic innervation of cortex by the basal forebrain: cytochemistry and cortical connections of the septal area, diagonal band nuclei, nucleus basalis (substantia innominata), and hypothalamus in the Rhesus monkey. *J. Comp. Neurol.* 214, 170–197.
- Mesulam, M.-M., Mufson, E., Wainer, B.H., 1986. Three-dimensional representation and cortical projection topography of the nucleus basalis (Ch4) in the macaque: concurrent demonstration of choline acetyltransferase and retrograde transport with a stabilized tetramethylbenzidine method for horseradish peroxidase. *Brain Res.* 367, 301–308.
- Morris, J.S., Friston, K.J., Dolan, R.J., 1998. Experience-dependent modulation of tonotopic neural responses in human auditory cortex. *Proc. R. Soc. Lond. B.* 265, 649–657.
- Morris, J.S., Friston, K.J., Dolan, R.J., 1997. Neural responses to salient visual stimuli. *Proc. R. Soc. Lond. B.* 264, 769–775.
- Morris, M.K., Bowers, D., Chatterjee, A., Heilman, K.M., 1992. Amnesia following a discrete basal forebrain lesion. *Brain* 115, 1827–1847.
- Mufson, E.J., Bothwell, M., Hersch, L.B., Kordower, J.H., 1988. Nerve growth factor receptor immunoreactive profiles in the normal, aged human basal forebrain: colocalization with cholinergic neurons. *J. Comp. Neurol.* 285, 196–217.
- Muir, J.L., Everitt, B.J., Robbins, T.W., 1994. AMPA-induced excitotoxic lesions of the basal forebrain: a significant role for the cortical cholinergic system in attentional function. *J. Neurosci.* 14, 2313–2326.
- Nadasdy, Z., Zaborszky, L., 2000. Computational analysis of spatial organization of large scale neural networks. *Anat. Embriol.* 204, 303–317.
- Nofzinger, E.A., Buysse, D.J., Miewald, J.M., Meltzer, C.C., Price, J.C., Sembrat, R.C., Ombao, H., Reynolds, C.F., Monk, T.H., Hall, M., Kupfer, D.J., Moore, R.Y., 2002. Human regional cerebral glucose metabolism during non-rapid eye movement sleep in relation to waking. *Brain* 125, 1105–1115.
- Paus, T., Zatorre, R.J., Hofle, N., Caramanos, Z., Gotman, J., Petrides, M., Evans, A.C., 1997. Time-related changes in neural systems underlying attention and arousal during the performance of an auditory vigilance task. *J. Cogn. Neurosci.* 9, 392–408.
- Pearson, R.C.A., Gatter, K.C., Brodal, P., Powell, T.P.S., 1983. The projection of the basal nucleus of Meynert upon the neocortex in the monkey. *Brain Res.* 259, 132–136.
- Perry, R.H., Candy, J.M., Perry, E.K., Thompson, J., Oakley, A.E., 1984. The substantia innominata and adjacent regions in the human brain: histochemical and biochemical observations. *Am. Anat.* 138, 713–732.
- Price, D.L., Whitehouse, P.J., Struble, R.G., 1986. Cellular pathology in Alzheimer's and Parkinson's diseases. *Trends Neurosci.* 9, 29–33.
- Reil, J.C., 1809. Untersuchungen über den Bau des grossen Gehirn im menschen. *Arch. Physiol. (Halle)* 9, 136–208.
- Richardson, R.T., DeLong, M.R., 1991. Electrophysiological studies of the functions of the nucleus basalis in primates. *Adv. Exp. Med. Biol.* 295, 233–252.
- Riedel, A., Hartig, W., Seeger, G., Gartner, U., Brauer, K., Arendt, T.H., 2002. Principles of rat subcortical forebrain organization: a study using histological techniques and multiple fluorescence labeling. *J. Chem. Neuroanat.* 23, 75–104.
- Rolland, P., Zilles, K., 1994. Brain atlases—A new research tool. *Trends Neurosci.* 17, 458–467.
- Sakamoto, N., Pearson, J., Shinoda, K., Alheid, G.F., de Olmos, J.S., Heimer, L., 1999. The human basal forebrain: Part I. An overview. In: Bloom, F.E., Bjorklund, A., Hokfelt, T. (Eds.), *The Primate Nervous System: Part III. Handbook of Chemical Neuroanatomy*, vol. 15. Elsevier, Amsterdam, pp. 1–55.
- Saper, C.B., 2004. Hypothalamus. In: Paxinos, G., Mai, J.K. (Eds.), *The Human Nervous System*, 2nd ed. Elsevier Academic Press, Amsterdam, pp. 514–550.
- Saper, C.B., Chelmsky, T.C., 1984. A cytoarchitectonic and histochemical study of nucleus basalis and associated cell groups in the normal human brain. *Neuroscience* 13, 1023–1037.
- Sarter, M., Gehring, W.J., Kozak, R., 2006. More attention must be paid: the neurobiology of attentional effort. *Brain Res. Rev.* 51, 145–1460.
- Sasaki, M., Ehara, S., Tamakawa, Y., Takahashi, S., Tohgi, H., Sakai, A., Mita, T., 1995. MR anatomy of the substantia innominata and findings in Alzheimer disease: a preliminary report. *AJNR Am. J. Neuroradiol.* 16, 2001–2007.
- Sesack, S.R., Deutch, A.Y., Bunney, B.S., 1989. Topographical organization of the efferent projections of the medial prefrontal cortex in the rat: an anterograde tract-tracing study with *Phaseolus vulgaris* *Leucoagglutinin*. *J. Comp. Neurol.* 290, 213–242.
- Schenker, C., Meier, D., Wichmann, W., Boesiger, P., Valavanis, A., 1993. Age distribution and iron dependency of the T2 relaxation time in the globus pallidus and putamen. *Neuroradiology* 35, 119–124.
- Schormann, T., Zilles, K., 1998. Three-dimensional linear and nonlinear transformations: An integration of light microscopical and MRI data. *Hum. Brain Map.* 6, 339–347.
- Spiga, S., Zaborszky, L., 2006. Connections between the medial prefrontal cortex and the basal forebrain: a combined anterograde–retrograde tracer study in rat. 236.4/E10 2006 Neuroscience Meeting Planner. Society for Neuroscience, Atlanta, GA. Online.
- Simic, G., Mrzljak, L., Fucic, A., Winblad, B., Lovric, H., Kostovic, I., 1999. Nucleus subputaminalis (Ayala): The still disregarded magnocellular component of the basal forebrain may be human specific and connected with the cortical speech area. *Neuroscience* 89, 73–89.
- Swaab, D.F., 2003. Nucleus basalis of Meynert (NBM) and diagonal band of Broca (DBB). In: Aminoff, M.J., Boller, F., Swaab, D.F. (Eds.), *The human hypothalamus: Basic and clinical aspects*, Part I, Vol. 79. Elsevier B. V., pp. 39–59.
- Swartz, B.E., Halgren, E., Fuster, J.M., Simpkins, F., Gee, M., Mandelkern, M., 1995. Cortical metabolic activation in humans during a visual memory task. *Cerebral Cortex* 5, 205–214.
- Talairach, J., Tournoux, P., 1988. *Co-planar Stereotaxic Atlas of the Human Brain*. Georg Thieme Verlag, Stuttgart.
- Teipel, S.J., Flatz, W.H., Heisen, H., Bokde, L.W., Schoenberg, S.O., Stockel, S., Dietrich, O., Reiser, M.F., Moller, H.-J., Hampel, H., 2005. Measurement of basal forebrain atrophy in Alzheimer's disease using MRI. *Brain* 128, 2626–2644.
- Turchi, J., Saunders, R.C., Mishkin, M., 2005. Effects of cholinergic deafferentation of the rhinal cortex on visual recognition memory in monkeys. *Proc. Natl. Acad. Sci. U.S.A.* 102, 2158–2161.
- Ulfing, N., 1989. Configuration of the magnocellular nuclei in the basal forebrain of the human adult. *Acta Anat.* 134, 100–105.
- Uylings, H.B.M., Zilles, K., Rajkowska, G., 1999. Optimal staining methods for delineation of cortical areas and neuron counts in human brains. *NeuroImage* 9, 439–445.
- Vogels, O.J.M., Broere, C.A.J., Ter Laak, H.J., Ten Donkelaar, H.J., Nieuwenhuys, R., Schulte, B.P.M., 1990. Cell loss and shrinkage in the nucleus basalis of Meynert complex in Alzheimer's disease. *Neurobiol. Aging* 11, 3–13.
- Voytko, M.L., Olton, D.S., Richardson, R.T., Gorman, L.K., Tobin, J.R., Price, D.L., 1994. Basal forebrain lesions in monkeys disrupt attention but not learning and memory. *J. Neurosci.* 14, 167–186.
- Wang, Y., Nakashima, K., Shiraishi, Y., Kawai, Y., Ohama, E., Takahashi, K., 1997. P300-like potential disappears in rabbits with lesions in the nucleus basalis of Meynert. *Exp. Brain Res.* 114, 288–292.
- Weinberger, N.M., 2007. Associative representational plasticity in the auditory cortex: a synthesis of two disciplines. *Learn. Mem.* 14, 1–16.
- Whitehouse, P.J., Price, D.L., Clark Jr., A.W., Coyle, J.T., DeLong, M.R., 1981. Alzheimer disease: evidence for selective loss of cholinergic neurons in the nucleus basalis. *Ann. Neurol.* 10, 122–126.
- Wilson, F.A., Rolls, E.T., 1990. Neuronal responses related to reinforcement in the primate basal forebrain. *Brain Res.* 509, 213–231.
- Zaborszky, L., 2002. The modular organization of brain systems. Basal forebrain: the last frontier. *Progr. Brain Res.* 136, 359–372.
- Zaborszky, L., Buhl, D.L., Pabalashingham, S., Bjaalie, J.G., Nadasdy, Z., 2005. Three-dimensional chemoarchitecture of the basal forebrain: spatially specific association of cholinergic and calcium binding protein-containing neurons. *Neuroscience* 136, 697–713.
- Zaborszky, L., Duque, A., 2003. Sleep–wake mechanisms and basal forebrain circuitry. *Front. Biosci.* 8, d1146–d1169 [PubMed#:12957822, URL: <http://www.bioscience.org>].
- Zaborszky, L., Pang, K., Somogyi, J., Nadasdy, Z., Kallo, I., 1999. The basal forebrain corticopetal system revisited. *Ann. NY. Acad. Sci.* 877, 339–367.
- Zilles, K., Schleicher, A., Palomero-Galalgher, N., Amunts, K., 2002. Quantitative analysis of cyto- and receptor architecture of the human brain. In: Toga, A.W., Mazziotta, J.C. (Eds.), *Brain Mapping: The Methods*. Academic Press, San Diego, pp. 573–602.